First measurement of the ^{33}Cl$(p,\alpha)^{30}$S reaction

C. M. Deibel,[1,2,*] K. E. Rehm,[2] J. M. Figueira,[3,2] J. P. Greene,[2] C. L. Jiang,[2] B. P. Kay,[2] H. Y. Lee,[2] J. C. Lighthall,[2,4] S. T. Marley,[2,4] R. C. Pardo,[2] N. Patel,[2,5] M. Paul,[6] C. Ugalde,[2,7,8] A. Woodard,[2] A. H. Wuosmaa,[4] and G. Zinkann[2]

[1]*Joint Institute for Nuclear Astrophysics, Michigan State University, East Lansing, Michigan 48824, USA*
[2]*Physics Division, Argonne National Laboratory, Argonne, Illinois 60439, USA*
[3]*Laboratorio Tandar, Comisión Nacional de Energía Atómica, B1650KNA San Martín, Buenos Aires, Argentina*
[4]*Physics Department, Western Michigan University, Kalamazoo, Michigan 49008, USA*
[5]*Department of Physics, Colorado School of Mines, Golden, Colorado 80401, USA*
[6]*Racah Institute of Physics, Hebrew University, Jerusalem, Israel*
[7]*Joint Institute for Nuclear Astrophysics, University of Chicago, Chicago, Illinois 60637, USA*
[8]*Department of Astrophysics and Astronomy, University of Chicago, Chicago, Illinois 60637, USA*

(Received 21 January 2011; revised manuscript received 6 April 2011; published 6 October 2011)

The ^{30}S$(\alpha,p)^{33}$Cl reaction may have a significant impact on final elemental abundances and energy output of type I X-ray bursts, as well as influencing observables such as double-peaked luminosity profiles, because it could bypass the ^{30}S waiting point. This reaction has been studied experimentally for the first time in inverse kinematics via the time-inverse reaction ^{1}H(^{33}Cl,^{30}S)α with a ^{33}Cl radioactive ion beam produced at the Argonne Tandem Linac Accelerator System facility by the "in-flight" technique. This reaction was studied at three different beam energies. The experimental method used and the resulting data are discussed.

DOI: 10.1103/PhysRevC.84.045802 PACS number(s): 26.30.Ca, 29.38.−c, 25.70.Hi

I. INTRODUCTION

Type I X-ray bursts (XRBs) are stellar events that occur in binary star systems containing a main sequence star orbiting and transferring H/He-rich matter onto a neutron star. As the pressure and density build up, the temperature increases and a thermonuclear runaway takes place. Peak temperatures reach $T_{\text{peak}} = 1$–2 GK. The duration of the bursts and their recurrence times vary, but typically bursts last 10–100 s, release 10^{39}–10^{40} ergs, and have recurrence times that range from a few hours to several days [1].

The nuclear flow is driven by the triple-α reaction, the (α,p) process, and hydrogen burning via the rapid-proton capture process (rp process) toward the proton-drip line [1,2]. As the nuclear flow occurs far from stability, there is little to no experimental information available on many of the reaction rates in these processes. As a result, models of XRBs depend largely on theoretical rates, which may be incorrect. However, there are a few reactions that still require radioactive beams but are located close enough to the valley of stability as to make them experimentally accessible. One of these is the ^{30}S$(\alpha,p)^{33}$Cl reaction, which has been shown to affect final elemental abundances and the energy output of XRBs [3].

In addition, ^{30}S is thought to be a waiting point during XRB nucleosynthesis (other potential waiting points in this mass region are ^{22}Mg, ^{26}Si, and ^{34}Ar) [4]. It has been suggested that the effects of this waiting point can be directly observed in so-called double-peaked luminosity profiles [5], which have been observed in several sources [6–8]. This paper is the first in a series that will examine the (α,p) reactions on potential intermediate-mass waiting-point nuclei using the method described in the following discussion.

Because both ^{30}S and ^{33}Cl as well as the compound nucleus ^{34}Ar are unstable, little is known about this reaction. Only one excited state in ^{34}Ar has been reported [9] within the Gamow window, which is located at an excitation energy of $E_0 \sim 8.6$ MeV with a width of approximately 0.9 MeV for a peak burst temperature of $\simeq$1 GK. While there have been recent efforts to obtain more experimental information on relevant states in ^{34}Ar [10], the ^{30}S$(\alpha,p)^{33}$Cl reaction has not been studied directly before. As a result, the ^{30}S$(\alpha,p)^{33}$Cl reaction rate used in XRB models so far is based only on theoretical rates.

In the following, an approach to experimentally measure this reaction by studying the time-inverse reaction in inverse kinematics, ^{1}H(^{33}Cl,^{30}S)α, is discussed. This time-inverse reaction was studied instead of the (α,p) reaction so that a solid CH_2 target could be used. Studying the reaction in inverse kinematics was necessary because ^{33}Cl has a short halflife (2.5 s) and therefore cannot be used as a target. Since beam intensities of only $\sim 10^4$ ^{33}Cl/s are available at current radioactive ion beam facilities, it was only possible, with the existing techniques described in Sec. II, to study this reaction at higher bombarding energies above the astrophysically relevant energy range. Therefore, this work should be considered a first step toward a determination of the reaction rate of ^{30}S$(\alpha,p)^{33}$Cl in XRBs. The development of a ^{33}Cl radioactive ion beam and a description of the general setup of the experiment are discussed in Sec. II. Sections III and IV focus on the determination of the ^{30}S$(\alpha,p)^{33}$Cl cross section and its implications for XRB nucleosynthesis, respectively.

II. EXPERIMENT

A. ^{33}Cl radioactive ion beam

The time-inverse reaction ^{33}Cl$(p,\alpha)^{30}$S was studied in inverse kinematics at the ATLAS facility at Argonne National

*Present address: Department of Physics and Astronomy, Louisiana State University, Baton Rouge, LA 70803, USA. deibel@phys.lsu.edu.

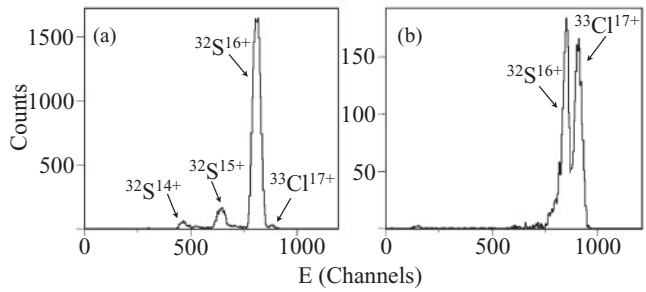

FIG. 1. Components of $^{32}S/^{33}Cl$ cocktail beam (a) without and (b) with the RF sweeper in use.

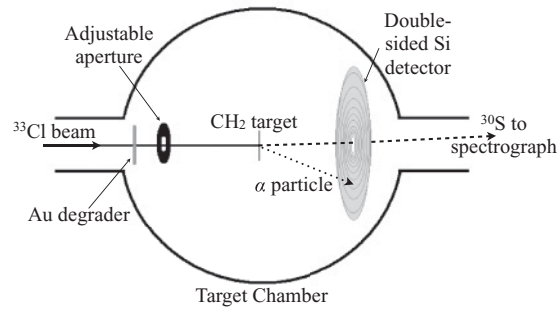

FIG. 2. Schematic of the experimental setup.

Laboratory using a radioactive ^{33}Cl beam. A ^{33}Cl beam was produced for the first time using the "in-flight" method, which is described in more detail in Ref. [11]. In this case, a 320-MeV primary beam (∼30–35 pnA) of stable $^{32}S^{13+}$ was incident on a gas cell, which was cryogenically cooled to −184 °C and filled with 1.4 atm of D_2 gas. The $d(^{32}S,^{33}Cl)n$ reaction produced the desired radioactive ^{33}Cl ions, which were emitted in a cone of $\leqslant 2.5°$. A ∼20 $\mu g/cm^2$ carbon stripping foil was located immediately following the gas cell to increase the charge state fraction of fully stripped $^{33}Cl^{17+}$. The ions were then focused with a superconducting solenoid and rebunched with a superconducting resonator. After a 22 ° bending magnet was used, a "cocktail" beam remained, which consisted mostly of the different charge states of the primary ^{32}S beam and the secondary $^{33}Cl^{17+}$ beam. These components were detected in a ΔE-E telescope consisting of two silicon surface barrier detectors located at the target position. While the ratio of ^{32}S to ^{33}Cl was on the order of 1000:1 [Fig. 1(a)], the species were well separated in time of flight. Therefore, a radio-frequency (RF) sweeper [12–14] was used to deflect as much of the primary beam as possible while allowing transmission of the main energy peak of the secondary beam, resulting in a much improved ^{32}S to ^{33}Cl ratio of approximately 1.4:1 [Fig. 1(b)]. The final beam consisted of the secondary $^{33}Cl^{17+}$ ions at 250 MeV and the low-energy tails of the primary beam's different charge states, which correspond to the magnetic rigidity allowed by the bending magnet ($^{32}S^{16+}$, $^{32}S^{15+}$, and $^{32}S^{14+}$ ions at 230, 202, and 176 MeV, respectively). The beam intensity at 250 MeV during the experiment was approximately 1.7×10^4 $^{33}Cl/s$ and varied by less than 5% during a 14-h-long measurement.

This 250-MeV ^{33}Cl beam was used for the first $^1H(^{33}Cl,^{30}S)\alpha$ measurement at the highest energy. Producing radioactive beams of this type is difficult and time-consuming, and changing the primary beam energy for lower-energy measurements would result in a prohibitively long experiment. Therefore, to lower the energy of the radioactive ion beam to 230 and 210 MeV, the original 250-MeV beam passed through Au degrader foils 4 and 8 mg/cm^2 thick, respectively. Because of the energy and small-angle straggling of the beam, the intensity for the 230- and 210-MeV beams was less by about a factor of two. The beam energies, nominally 250, 230, and 210 MeV, were experimentally determined to be 250.6(13), 229.1(13), and 208.1(14) MeV, respectively, using a split-pole magnetic spectrograph whose focal plane detector was calibrated with a ^{228}Th α source.

B. Experimental Setup

As shown in Fig. 2, the beam was incident on a 650 $\mu g/cm^2$ CH_2 target. The α particles were detected in a 1000-μm-thick annular double-sided Si detector[1] (DSSD) with a back plane segmented into 16 wedges and a front plane divided into 16 rings segmented in θ_{lab}. The detector was placed such that the 16 rings covered an angular range of $\theta_{lab} = 8$–$25°$ with respect to the target. The ^{30}S reaction products were separated from the main beam (^{33}Cl and ^{32}S), and other reaction products by an Enge split-pole magnetic spectrograph. The particles were detected by an xy position-sensitive parallel grid avalanche counter (PGAC) and ionization chamber (IC) located at the focal plane of the spectrograph and filled with 5 Torr of isobutane and 15 Torr of CF_4 gas, respectively. The PGAC measured the time of flight and the focal-plane position (or magnetic rigidity) of the particles, and the IC gave the energy loss in the gas, allowing rudimentary particle identification. Detecting the ^{30}S reaction products in coincidence with the α particles detected in the DSSD was necessary because elastically scattered beam particles were also detected in the DSSD. Without a coincidence requirement, the DSSD spectrum was overwhelmed by the scattered beam, which was orders of magnitude more intense than the α particles resulting from the (p, α) reaction.

C. Gas-filled spectrograph method

The Enge split-pole magnetic spectrograph was located at 0° for the measurement. When the spectrograph is operated in vacuum mode, the ^{30}S reaction products are dispersed according to their charge state distribution along the focal plane, and because of the finite momentum acceptance, not all of the ^{30}S reaction products of interest are detected at the focal plane. In addition, the charge state distributions of different ion groups overlap, making it impossible to block the higher intensity primary beam particles without also blocking some of the reaction products of interest. The spectrograph was therefore run in "gas-filled mode" [15,16], where a 1.3 mg/cm^2

[1]Micron Semiconductor Ltd. model S2.

Ti window separated the target chamber from the spectrograph, which was filled with 15, 11, and 9 Torr of N_2 gas for the 250, 230, and 210 MeV runs, respectively. The charge-exchange collisions of the reaction products with the N_2 gas resulted in all particles of a specific species convening to a mean charge state. While this method has the drawback of decreasing the resolution because of energy and angle straggling, any loss of ions due to the charge state distribution is avoided, which is critical in these low-statistics experiments. Furthermore, a spatial separation of the ^{30}S recoils from the ^{32}S and ^{33}Cl beams can be achieved because particles are separated in first order in the focal plane according to their $m\overline{v}/\overline{q}$, where the mean charge state $\overline{q}$ depends on $(v/v_0)^{\delta}Z^{-\gamma}$, where v_0 is the Bohr velocity, $\delta = 0.6$, and $\gamma = 0.61$ [16]. Further details of this technique using stable beams are described in Refs. [15–20].

III. ANALYSIS AND RESULTS

The yield of the (p,α) reaction was determined by the number of α particles detected in the DSSD in coincidence with the ^{30}S reaction products detected at the focal plane of the spectrograph. The timing peak resulting from these coincidences, which represents ^{30}S and α particles that result from a ^{1}H(^{33}Cl,^{30}S)α reaction, was used to eliminate most of the background in the DSSD. As the energy and small-angle straggling due to the Ti foil and the N_2 gas in the spectrograph resulted in a diffuse particle group in the focal plane position versus time-of-flight spectrum, a wide particle identification gate was used to eliminate some of the remaining background. This cut is needed because of the large amount of scattered beam, as shown in Fig. 3(a). While the coincidence condition eliminates much of this residual beam, there still exists some background associated with higher energy particles detected in the DSSD [Fig. 3(b)], which is eliminated by this cut.

Because more than half of the beam used was ^{32}S, contaminants from the ^{1}H(^{32}S,^{29}P)α reaction were a concern. Therefore, data were also taken with a pure ^{32}S beam. The resulting α-^{29}P coincidences yielded no discernible kinematic curve when measured at the highest beam energy used, which is expected based on a predicted cross section of over an order of magnitude smaller than that for ^{1}H(^{33}Cl,^{30}S)α [21–23]. Calculations also show that any α particles detected resulting from either the ^{1}H(^{32}S,^{29}P)α reaction or reactions between the beam and the carbon component of the target would be well separated from the α particles of interest produced by the ^{1}H(^{33}Cl,^{30}S)α reaction (see Fig. 4). Any contributions to the background from other light ion reactions do not pose a problem as those reactions [e.g., (p,d), (p,t), and $(p,^{3}\mathrm{He})$] are energetically forbidden. Furthermore, a background subtraction was done for coincidences due to contaminants and/or any random coincidences by gating on the background of the coincidence timing spectrum to determine the background in the DSSD coincidence spectrum.

The experimental result, shown in Fig. 5, is the expected kinematic curve of the angle of emittance of the α particles as a function of their energy detected in the DSSD. The thickness of the DSSD was not sufficient to stop α particles with energy greater than approximately 48 MeV. The energy deposited

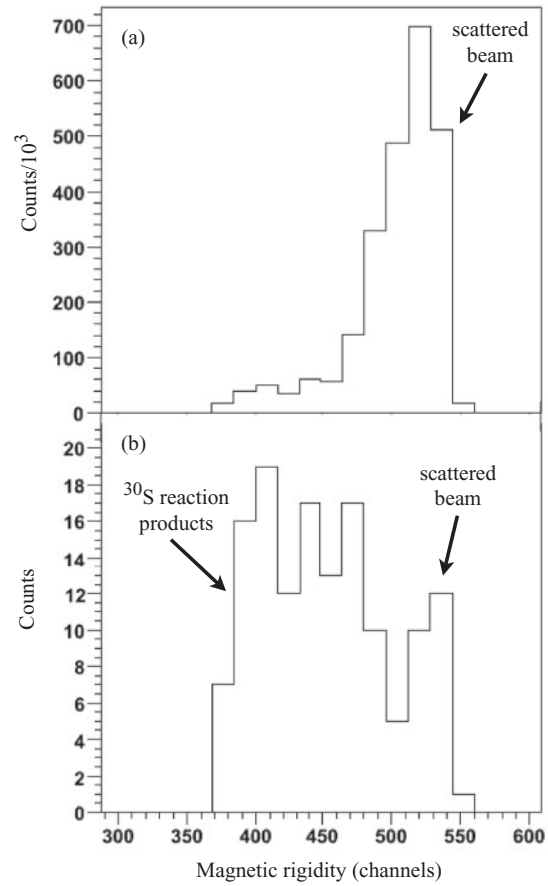

FIG. 3. Focal plane position, or magnetic rigidity, of particles detected at the focal plane of the spectrograph for (a) the raw data and (b) particles associated with the energy range of interest for particles detected in the DSSD ($E \geqslant 20$ MeV) that also satisfy the coincidence condition. Peaks resulting from the scattered beam and the particle group of interest are shown.

in the DSSD by these α particles decreases with increasing α-particle energy and results in a "kink" in the θ_{lab} versus energy spectrum for the kinematic curve associated with the ground state of ^{30}S, as can be seen in the lower right-hand corners of Figs. 4 and 5.

A. Normalization

Several efficiency corrections to the yield of the α particles of interest were needed to determine the reaction cross section. The DSSD only spanned a range of 8° to 25° in the laboratory frame of reference, while the α particles from the (p,α) reaction have a maximum angle of $\theta_{\mathrm{lab}} = 24°$; therefore, any α particles emitted between 0° and 8° were not detected. As the beam spot had a diameter of 7.5 mm, α particles with a given energy and emission angle could be detected in one of several rings, resulting in the spread of the kinematic curve shown in Fig. 5. This also meant that some of the α particles emitted at the largest angles were not detected. This can be seen from the sharp cutoff at the largest angles in Fig. 5 and is taken into account in the correction for the geometrical efficiency of

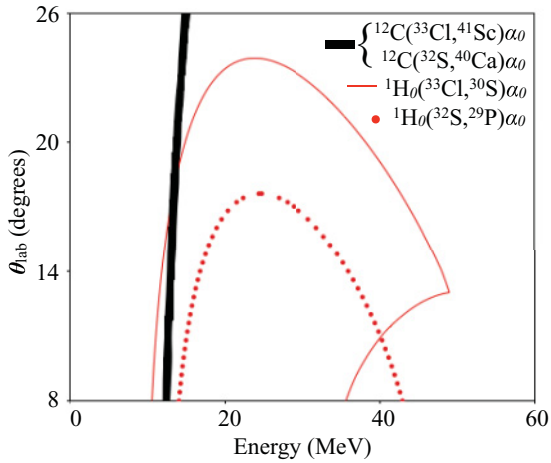

FIG. 4. (Color online) Kinematic calculations of θ_{lab} as a function of α-particle energy from the $^{1}H_0(^{33}Cl,^{30}S)\alpha_0$ reaction of interest (solid, thin line; red online), contaminants from the $^{1}H_0(^{32}S,^{29}P)\alpha_0$ reaction (dots; red online), and contaminants from the $^{12}C(^{33}Cl,^{41}Sc)\alpha_0$ and $^{12}C(^{32}S,^{40}Ca)\alpha_0$ reactions (broad black line). The contaminant α particles are well separated from the high-energy branch of the α particles of interest from the $^{1}H_0(^{33}Cl,^{30}S)\alpha_0$ reaction (see text for more details).

the DSSD. Furthermore, only the high-energy α branch of the θ_{lab} versus energy distribution was detected, because the ^{30}S reaction products associated with the low-energy α branch had the same average magnetic rigidity as the ^{33}Cl beam particles, which were blocked from entering the PGAC to avoid high counting rates. For the 250-MeV measurement, Monte Carlo simulations gave a geometrical detection efficiency of 82% for the DSSD and calculated that 67% of the total α-particle

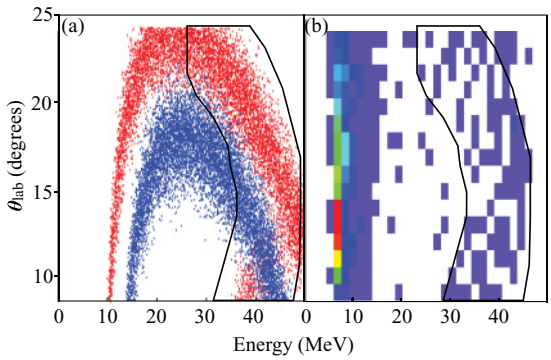

FIG. 5. (Color online) Kinematic curves of the laboratory angle as a function of energy of α particles detected in the DSSD for a ^{33}Cl beam of 250 MeV from (a) a Monte Carlo simulation and (b) data gated on the coincidence timing peak and the ^{30}S particle group for the $^{1}H(^{33}Cl,^{30}S)\alpha$ reaction. In (a), the outer curve (red online) represents the α particles associated with the ground state of ^{30}S, which is outlined, and the inner curve (blue online) describes the α particles associated with the first excited state ($E_x = 2.21$ MeV) of ^{30}S and is well separated from the ground state. In (b), the α kinematic curve is outlined with the same shape as shown in (a). The strong particle group at low energies seen in (b) originates from inelastically scattered protons from the target.

yield was in the high-energy branch, assuming an isotropic angular distribution in the center-of-mass frame. While the assumption of an isotropic distribution may not be realistic, stable beam runs using the same experimental setup [18–20] show that the effects from nonisotropic distributions are washed out in the angle-integrated cross sections. Finally, the Monte Carlo simulation determined that the aperture of the split-pole spectrograph accepted only 38% of the ^{30}S particles emitted from the reaction. The α-particle yield was corrected accordingly. The uncertainty in the Monte Carlo calculations was on the order of a few percent, which was added in quadrature with the other uncertainties in the calculation of the cross section.

To determine the cross section, the total beam dosage and the amount of ^{1}H in the target had to be measured. This was done in two ways. At the greatest ^{33}Cl beam energy of 250 MeV, the Rutherford scattering yield N_{Ruth} of the beam on the C component of the CH_2 target was measured at $\theta_{lab} = 2.5^\circ$ in the spectrograph [24]. The elastic-scattering yield N_{el} of the recoil protons from the CH_2 target could be detected in the DSSD at angles of $\theta_{lab} \simeq 8^\circ$–$9^\circ$ during the Rutherford scattering measurement. The same recoil yield, $N_{el,run}$ could be measured throughout the 250-MeV measurement to monitor the beam current and target composition, and by using the known ratio N_{Ruth}/N_{el}, the cross section of the $^{1}H(^{33}Cl,^{30}S)\alpha$ reaction at 250 MeV could be normalized via the expression

$$\sigma_{(p,\alpha)} = N_\alpha \times \Omega_{PGAC} \times \frac{N_{el}}{N_{Ruth}} \left(\frac{d\sigma}{d\Omega}\right)_{Ruth} \frac{1}{N_{el,run}} \frac{1}{2\eta_{MC}}, \quad (1)$$

where Ω_{PGAC} is the solid angle acceptance of the spectrograph, η_{MC} is the efficiency factor determined by the Monte Carlo simulations discussed previously, $N_{el,run}$ is the yield of the recoil protons during the entire 250-MeV run, $(\frac{d\sigma}{d\Omega})_{Ruth}$ is the Rutherford cross section for ^{33}Cl on ^{12}C at 2.5°, and N_α is the α-particle yield from the reaction of interest during the run. The factor of 2 accounts for the fact that the Rutherford scattering is from the carbon component of the target, which has a 1:2 ratio with the hydrogen component.

The angular dependence of the Rutherford cross section at small angles introduced a large uncertainty (more than 50%) to this method of normalization, as the aperture to the spectrograph had a finite width of $\theta_{lab} = 1.5^\circ$. Therefore, a second method of beam normalization was used. Approximately every 2 h during the experiment, the magnetic field of the spectrograph was changed and the beam intensity was attenuated by a factor of 10^3 so that the beam could be measured directly at the focal plane of the spectrograph. Monte Carlo simulations show that approximately 95% of the beam passed through the aperture of the spectrograph during these direct beam measurement runs. These losses are caused by the ~7.5-mm-radius beam spot and the straggling of the beam when degraders were used. The beam intensity varied by less than 5% for the 250-MeV beam energy over a period of 14 h. Cross sections determined using this beam monitoring method agreed within uncertainties with those found using the Rutherford normalization method discussed previously.

At lower beam energies where the beam was degraded by Au foils, only this latter method of normalization was used, as the straggling induced by those foils severely broadened the peak of the recoil protons detected in the DSSD. For the degraded beams, the variations in beam intensities were larger than for the direct beam ($\leqslant$30% over 20 h and $\leqslant$13% over 19 h for the 230- and 210-MeV beams, respectively). These variations were the largest source of uncertainty for the degraded beam measurements.

B. Cross sections

As the ^{33}Cl beam was in its ground state, any contributions to the ^{30}S$(\alpha,p)^{33}$Cl reaction rate populating excited states in the residual ^{33}Cl nucleus are not taken into account. A study of the ^{33}Cl$(p,p')^{33}$Cl reaction would be necessary to measure any such contribution. Therefore, the measured cross sections discussed are for the ground-state to ground-state transitions only: ^{33}Cl$(p_0,\alpha_0)^{30}$S and ^{30}S$(\alpha_0,p_0)^{33}$Cl.

The cross sections for the ^{33}Cl$(p_0,\alpha_0)^{30}$S reaction at each center-of-mass energy are given in Table I along with the cross sections for the corresponding ^{30}S$(\alpha_0,p_0)^{33}$Cl reaction determined via the reciprocity theorem [2]. The uncertainties in the cross sections are dominated by the uncertainty in the beam currents discussed previously. Additionally, there was a 10% uncertainty originating from the background in the DSSD α-^{30}S coincidence spectra. These two errors, the uncertainty from the Monte Carlo simulations, and the statistical error were added in quadrature to determine the final uncertainties in the cross sections normalized via beam monitoring. The 250-MeV measurement normalized using Rutherford scattering includes the statistical and systematic errors associated with the particle yields in the uncertainty of the cross section, as well as the uncertainty from the Rutherford cross section resulting from the finite opening of the aperture to the spectrograph. The cross sections shown in Table I for this highest beam energy are weighted averages of these two methods of normalization. Because the measurement is for ground-state to ground-state transitions only, as discussed previously, the cross sections given in Table I represent lower limits of the (p_0,α) and (α_0,p) reaction cross sections.

TABLE I. Cross sections for the ^{33}Cl$(p_0,\alpha_0)^{30}$S and ^{30}S$(\alpha_0,p_0)^{33}$Cl reactions for each beam energy and the corresponding center-of-mass (c.m.) energy.

Beam energy (MeV)			Cross sections (mb)	
Laboratory	c.m. (p_0,α_0)	c.m. (α_0,p_0)	Measured (p_0,α_0)	Converted (α_0,p_0)
250.6(13)	7.43(4)	5.35(4)	7.1(13)[a]	21.8(40)[a]
229.1(13)	6.79(4)	4.71(4)	11.8(40)	37.8(128)
208.1(14)	6.17(4)	4.09(4)	1.3[b]	4.5[b]

[a]Weighted average of cross sections found using two different methods of normalization (see text).
[b]Upper limit.

IV. CONCLUSIONS

The cross sections measured in this experiment are compared with the theoretical predictions of the NON-SMOKER code calculations [21–23] in Fig. 6. As seen in Fig. 6, the experimentally determined cross sections for the ^{33}Cl$(p_0,\alpha_0)^{30}$S reaction are approximately a factor of four or more greater than those predicted by NON-SMOKER, which include contributions from transfer to excited states in ^{30}S. As seen in Fig. 5, those contributions were experimentally found to be small. Indeed, calculations of the ^{33}Cl$(p_0,\alpha)^{30}$S cross section show that the reaction is dominated by transitions to the ground state in ^{30}S and that the ^{33}Cl$(p_0,\alpha_0)^{30}$S cross section is approximately equal to the ^{33}Cl$(p_0,\alpha)^{30}$S cross section [25]. As both the ^{33}Cl beam and the final ^{30}S nuclei are in their ground states, the reciprocity theorem was used to convert the experimental ^{33}Cl$(p_0,\alpha_0)^{30}$S cross sections to the ^{30}S$(\alpha_0,p_0)^{33}$Cl cross sections. These converted cross sections, shown in Table I, are close to the NON-SMOKER calculations of the ^{30}S$(\alpha_0,p)^{33}$Cl reaction. This is because the theoretical calculations include transitions to excited states in the residual ^{33}Cl nucleus, which have a larger contribution in the forward (α_0,p) reaction compared to the contributions to the inverse (p_0,α) reaction from excited states in ^{30}S [25]. As the experimental cross sections given in Table I do not include these transitions and thus represent lower limits, the ^{30}S$(\alpha_0,p)^{33}$Cl reaction cross section may be larger than predicted. In addition, the compound nucleus ^{34}Ar is at the limit of the region where the statistical Hauser-Feshbach model can be applied, and the ^{30}S$(\alpha_0,p)^{33}$Cl reaction may be dominated by resonances [21,22,25] that are unknown because of the limited data on the level structure of ^{34}Ar. As a result, a comparison of the measured ^{30}S$(\alpha_0,p_0)^{33}$Cl reaction (or of a future measurement that includes transitions to excited states in ^{33}Cl) with the

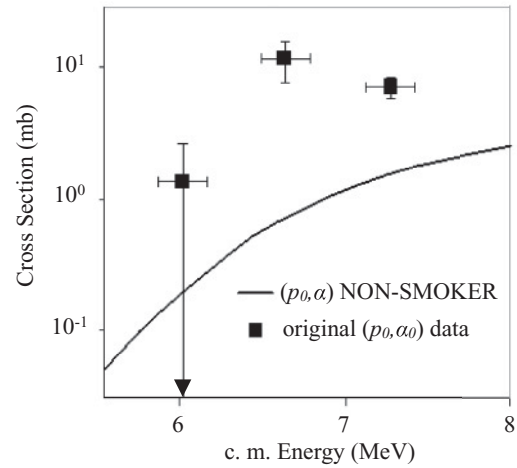

FIG. 6. Cross section as a function of c.m. energy for the ^{33}Cl$(p_0,\alpha_0)^{30}$S data (squares) and the NON-SMOKER calculations [21–23] for the ^{33}Cl$(p_0,\alpha)^{30}$S cross section (solid line). The experimental data include only ground-state to ground-state transitions, while the NON-SMOKER calculations include transitions to excited states (see text for details). The vertical error bars indicate the uncertainties in the cross sections, and the horizontal error bars indicate the energy spread of the beam in the target.

^{30}S$(\alpha_0, p)^{33}$Cl reaction calculated using the NON-SMOKER code or other Hauser-Feshbach theoretical methods may not be meaningful, and the same is true for the inverse ^{33}Cl$(p_0,\alpha_0)^{30}$S reaction. Furthermore, these measurements should not be extrapolated to the astrophysically relevant energy regime, because of the likely resonant structure of the cross section excitation function.

The work described here is above the energy range of interest in XRBs (which is in the region $E_{cm} = 3.5$–4.4 MeV for the ^{1}H(^{33}Cl,^{30}S)α reaction), and data at ^{33}Cl beam energies between 120 and 150 MeV are needed. Currently, only beam intensities of $\sim 10^4$ ^{33}Cl/s are available at ATLAS, making measurements at these lower energies impossible. However, improvements to the in-flight radioactive beam facility are under development, which should lead to further increases in beam intensity. In the meantime, excited states within the Gamow window in the compound nucleus ^{34}Ar are being studied via indirect methods [10] to improve the nuclear structure information involved in calculations of the ^{30}S$(\alpha, p)^{33}$Cl reaction rate, which is needed given the limits of theoretical calculations discussed previously.

Ideally, this reaction should be studied directly using a ^{30}S beam impinging upon a ^{4}He target, and plans to do so using the new HELIOS device at ATLAS [26,27] are being explored. The (α, p)-reaction rates on the other possible waiting points in this mass region, ^{22}Mg, ^{26}Si, and ^{34}Ar, also need to be measured. The reaction rates on these waiting-point nuclei can then be used in XRB models to study their effects on XRB nucleosynthesis and energy generation. This work represents first step toward the determination of the astrophysical reaction rate of ^{30}S$(\alpha, p)^{33}$Cl in XRBs, which could have significant influence on the elemental and energy production in these events that can be directly compared with theoretical models.

ACKNOWLEDGMENTS

This work has been supported by JINA Grant No. PHY0822648 and the US DOE Contract No. DE-AC02-06CH11357. We also thank T. Rauscher for helpful discussions of the NON-SMOKER calculations and the ATLAS operations staff for making this study possible.

[1] H. Schatz and K. E. Rehm, Nucl. Phys. A **777**, 601 (2006).
[2] C. Iliadis, *Nuclear Physics of Stars* (Wiley-VCH Verlag, Weinheim, 2007), p. 31.
[3] A. Parikh, J. José, F. Moreno, and C. Iliadis, Astrophys. J. Suppl. Ser. **178**, 110 (2008).
[4] J. L. Fisker, H. Schatz, and F.-K. Thielemann, Astrophys. J. Suppl. Ser. **174**, 261 (2008).
[5] J. L. Fisker, F. K. Thielemann, and M. Wiescher, Astrophys. J. Lett. **608**, 61 (2004).
[6] M. Sztajno, J. van Paradijs, W. H. G. Lewin, J. Trümper, G. Stollman, W. Pietsch, and M. van der Klis, Astrophys. J. **299**, 487 (1985).
[7] W. Penninx, J. van Paradijs, and W. H. G. Lewin, Astrophys. J. Lett. **321**, 67 (1987).
[8] E. Kuulkers, J. Homan, M. van der Klis, W. H. G. Lewin, and M. Méndez, Astron. Astrophys. **382**, 947 (2002).
[9] P. M. Endt, Nucl. Phys. A **633**, 1 (1998).
[10] S. O'Brien *et al.* in *Capture Gamma-Ray Spectroscopy and Related Topics: 13th International Symposium*, edited by N. W. A. Blazhev, J. Jolie, and A. Zilges (American Institute of Physics, 2009), p. 288.
[11] B. Harss *et al.* Rev. Sci. Instrum. **71**, 380 (2000).
[12] K. E. G. Löbner, U. Lenz, U. Quade, K. Rudolph, W. Schomburg, S. J. Skorka, and M. Steinmayer, Nucl. Instrum. Methods B **26**, 301 (1987).
[13] D. Bazin, V. Andreev, A. Becerril, M. Doléans, P. F. Mantica, J. Ottarson, H. Schatz, J. B. Stoker, and J. Vincent, Nucl. Instrum. Methods A **606**, 314 (2009).
[14] R. C. Pardo *et al.* (in preparation).
[15] M. Paul, B. G. Glagola, W. Henning, J. G. Keller, W. Kutschera, Z. Liu, K. E. Rehm, B. Schneck, and R. H. Siemssen, Nucl. Instrum. Methods A **277**, 418 (1989).
[16] K. E. Rehm *et al.*, Nucl. Instrum. Methods A **370**, 438 (1996).
[17] J. M. Figueira *et al.* (in preparation).
[18] J. M. Figueira *et al.* AIP Conf. Proc. **1265**, 174 (2010).
[19] J. M. Figueira *et al.* (in preparation).
[20] J. M. Figueira, Ph.D. thesis, Laboratorio Tandar, Comisión Nacional de Energía Atómica, 2011 (in preparation).
[21] T. Rauscher and F.-K. Thielemann, At. Data Nucl. Data Tables **75**, 1 (2000).
[22] T. Rauscher and F.-K. Thielemann, At. Data Nucl. Data Tables **79**, 47 (2001).
[23] T. Rauscher, computer code NON-SMOKER, [http://nucastro.org/nonsmoker.html]
[24] S. Pirrone, S. Aiello, N. Arena, S. Cavallaro, S. Femino, G. Lanzalone, G. Politi, F. Porto, S. Romano, and S. Sambataro, Phys. Rev. C **55**, 2482 (1997).
[25] T. Rauscher (private communication).
[26] A. H. Wuosmaa, J. P. Schiffer, B. B. Back, C. J. Lister, and K. E. Rehm, Nucl. Instrum. Methods A **580**, 1290 (2007).
[27] J. C. Lighthall *et al.*, Nucl. Instrum. Methods A **622**, 97 (2010).